EDGE ARTICLE

CrossMark
click for updates

Electrostatic binding of polyanions using self-assembled multivalent (SAMul) ligand displays – structure–activity effects on DNA/heparin binding†

Loryn E. Fechner,[a] Buthaina Albanyan,[a] Vânia M. P. Vieira,[a] Erik Laurini,[b] Paola Posocco,[b] Sabrina Pricl*[b] and David K. Smith*[a]

This paper reports that modifying the ligands in self-assembled multivalent (SAMul) displays has an impact on apparent binding selectivity towards two nanoscale biological polyanions – heparin and DNA. For the nanostructures assayed here, spermidine ligands are optimal for heparin binding but spermine ligands are preferred for DNA. Probing subtle differences in such nanoscale binding interfaces is a significant challenge, and as such, several experimental binding assays – competition assays and isothermal calorimetry – are employed to confirm differences in affinity and provide thermodynamic insights. Given the dynamic nature and hierarchical binding processes involved in SAMul systems, we employed multiscale modelling to propose reasons for the origins of polyanion selectivity differences. The modelling results, when expressed in thermodynamic terms and compared with the experimental data, suggest that DNA is a shape-persistent polyanion, and selectivity originates only from ligand preferences, whereas heparin is more flexible and adaptive, and as such, actively reinforces ligand preferences. As such, this study suggests that inherent differences between polyanions may underpin subtle binding selectivity differences, and that even simple electrostatic interfaces such as these can have a degree of tunability, which has implications for biological control and regulation on the nanoscale.

Introduction

Biology is dominated by polyanions, such as nucleic acids, glycosaminoglycans, proteoglycans, micro-tubules and membranes – subtle discrimination between these nanoscale species is important to regulate and control this 'polyanion world'.[1] However, discrimination between polyanions is a highly challenging target given their similarities in terms of charge density, their charge providing the primary mechanism by which they can be bound. As such, in terms of supramolecular and nanoscale chemistry, polyanions are interesting, but difficult targets for selective binding. As a result, most studies focus on a specific anion with a defined application in mind, *e.g.*, DNA binding for gene delivery,[2] or heparin binding for coagulation control.[3] The development of active agents in these two areas is of considerable clinical relevance and has made these polyanions of great interest. Considering these two specific anions,

DNA is a negatively charged as a result of phosphate links in the sugar backbone, while the polysaccharide backbone of heparin is appended with anionic sulfates and carboxylates. Clearly there are some inherent differences between these polyanions, but surprisingly, there has been relatively little interest in probing binding selectivity. Obviously, if we could understand the factors which allow receptors to preferentially bind to one polyanion over another, as well as addressing a genuine challenge in supramolecular design, we would also be able to develop systems that are able to intervene much more precisely in processes of biomedical relevance and are better optimised for specific clinical applications.[2,3]

Nanoscale targets such as polyanions are also a significant challenge for supramolecular chemistry because of their relatively large, solvent-exposed surfaces.[4] Effective binding is best achieved using multivalency, *i.e.*, employing ligands with many points of interaction.[5] Given the relative difficulty of using synthetic chemistry to construct covalent multivalent arrays, there has recently been increasing interest in developing self-assembled multivalent (SAMul) ligand displays, in which multiple ligands non-covalently assemble to generate a nanoscale display which interacts with a binding partner.[6] This hierarchical approach to nanoscale recognition has been used to target (*e.g.*) sugar binding proteins,[7] integrins,[8] nucleic acids[9] and heparin.[10] SAMul is a tunable strategy because it only requires the synthesis of small molecules – it is therefore easy to

[a] Department of Chemistry, University of York, Heslington, York, YO10 5DD, UK. E-mail: david.smith@york.ac.uk

[b] Simulation Engineering (MOSE) Laboratory, Department of Engineering and Architectures (DEA), University of Trieste, Trieste, 34127, Italy. E-mail: sabrina.pricl@di3.units.it

† Electronic supplementary information (ESI) available: Full synthetic methods and characterisation data, assay and modelling methodologies, further experimental data from binding assays, DLS and TEM. See DOI: 10.1039/c5sc04801j

introduce structural variation and explore structure–activity relationships. To bind polyanions such as DNA or heparin requires cationic ligands,[9,10] which bind *via* multiple electrostatic ion–ion interactions. We recently reported that ligand chirality could influence apparent heparin/DNA binding selectivity,[11] but selective polyanion binding, for the reasons outlined above, remains a rarely explored, challenging target.

There has been considerable interest in colloid science in investigating the interaction of self-assembled simple cationic lipids with specific polyanions in both practical and theoretical terms.[12] In the widely accepted model, charge density plays the dominant role in binding – it is noted that other interactions can then influence selectivity, but there are relatively few specific experimental examples of this.[13] Synthetic polyanions have been studied, and it has been shown, for example, that hydrophobic interactions between the polymer chain and the hydrophobic unit in the lipid can play an important role in moderating charge–charge binding effects.[14] In this paper, we determine the impact of ligand choice in our SAMul displays and report an experimental example in which we uncover apparent selectivities of naturally occurring biopolyanions, DNA and heparin, for different nanoscale assemblies – we use multiscale modelling methods to provide further insight into the complex, interdependent, hierarchical self-assembly and nanoscale binding processes.

Results and discussion

For the purposes of this structure–activity effect study, amphiphilic molecules with different ligands were synthesised (Fig. 1) each of which could, in principle, self-assemble into micelles displaying cationic ligand surfaces. As hydrophobe we selected palmitic acid (C_{16}), with different amines as ligands, connected using TBTU-mediated peptide coupling with an appropriate protecting group strategy (see ESI†). This yielded C_{16}-DAP, C_{16}-DAPMA, C_{16}-SPD and C_{16}-SPM, with nominal ligand charges of +1, +2, +2 and +3 respectively at physiological pH (7.4). Singly-charged C_{16}-DAP was largely insoluble in water/buffer – its +1 charge is insufficient to counterbalance the hydrophobicity, and it was not studied further. Compound C_{16}-DAPMA (+2) had good aqueous solubility, spermidine-based C_{16}-SPD (+2) was slightly less soluble, and spermine-derived C_{16}-SPM (+3) was more difficult to dissolve. We reason the +3 charge of C_{16}-SPM hinders assembly, and hence solubility, because cation–cation

repulsions on the micellar surface are not fully offset by the hydrophobic driving force for assembly.[15]

We initially quantified self-assembly using a Nile Red assay[16] in 150 mM NaCl. All studies in this paper were performed at this salt concentration; ionic strength can have a major impact on electrostatic binding and it is important to keep it constant. The resulting critical micelle concentrations (CMCs) supported the macroscopic solubility observations, with C_{16}-DAPMA having the lowest CMC and C_{16}-SPM the highest, with C_{16}-SPM requiring heating to encourage solubility – in agreement with entropically-driven hydrophobic self-assembly. Further analysis of CMC data in different buffer/salt conditions is provided in the ESI.† For validation, we also used isothermal titration calorimetry (ITC) and the resulting CMCs were in very good agreement with those from the Nile Red assay (Table 1). Importantly, treatment of the ITC data also provided thermodynamic parameters for self-assembly (ΔH_{mic}, $T\Delta S_{mic}$ and ΔG_{mic}) which support the proposal that C_{16}-SPM had the least favourable self-assembly, primarily as a result of the enthalpic term. Dynamic light scattering (DLS, Fig. S1–S3,† Table 1) indicated, based on the volume contribution, that all three compounds formed similar-sized assemblies, as may be expected given the relatively similar molecular sizes of the three compounds. Perhaps surprisingly, the most highly-charged C_{16}-SPM actually formed the assembly with the lowest zeta potential – significantly lower than that observed for C_{16}-DAPMA, which may reflect the difficulty of bringing these more highly charged ligands into close proximity on the nanoscale surface. We also used transmission electron microscopy (TEM) to visualise the self-assembled nanostructures formed by these ligands (Fig. S4–S6†). On drying aqueous samples on a TEM grid, we observed that in each case, self-assembled spherical nanostructures could be visualised, in good general agreement with the DLS data.

To further understand self-assembly, we used multiscale molecular simulation in 150 mM aqueous NaCl (see ESI†).[17] Spherical micelles were obtained in all cases (*e.g.*, Fig. 2). Interestingly, simulation indicated that the compounds formed micelles with different packing densities. Specifically, the aggregation number (N_{agg}, Table 2) suggests that C_{16}-DAPMA

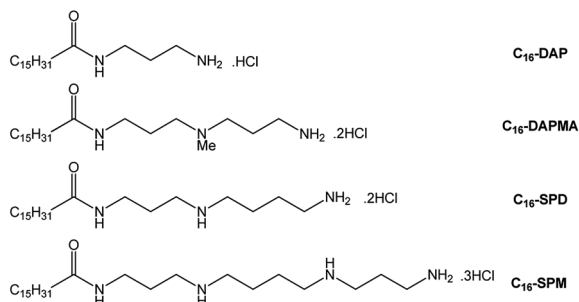**Table 1** Critical Micelle Concentrations (CMCs) for compounds in 10 mM Tris buffer (with 150 mM NaCl) determined by Nile Red (CMC^{NR}) and ITC-derived thermodynamic data of micellisation (CMC^{ITC}) and zeta sizing data (from DLS based on the volume contribution). $\Delta G_{mic} = \Delta H_{mic} - T\Delta S_{mic}$, where ΔG_{mic}, ΔH_{mic}, and $T\Delta S_{mic}$ are the free energy, enthalpy and entropy of micellisation, respectively

	C_{16}-DAPMA (+2)	C_{16}-SPD (+2)	C_{16}-SPM^a (+3)
CMC^{NR}/μM	40 ± 1	51 ± 2	65 ± 20
CMC^{ITC}/μM	34	52	71
ΔH_{mic}/kJ mol^{-1}	−10.81	−8.61	−8.41
$T\Delta S_{mic}$/kJ mol^{-1}	14.72	15.86	15.29
ΔG_{mic}/kJ mol^{-1}	−25.52	−24.47	−23.70
Diameter/nm	6.2 ± 1.3	6.6 ± 0.2	6.2 ± 0.1
Zeta potential/mV	+51.9 ± 2.6	+44.0 ± 1.7	+40.5 ± 0.9

^{a} Heating was required to encourage solubility under these conditions.

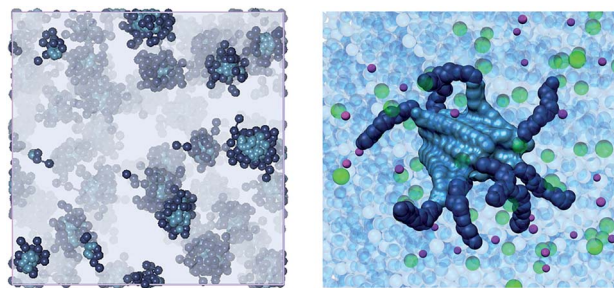Fig. 1 Compounds investigated in this paper.

Fig. 2 Mesoscopic (left) and atomistic (right) simulations of C_{16}-SPM self-assembling into micelles. The C_{16} hydrophobic portion is shown as steel blue spheres whereas the SPM residues are portrayed as navy blue spheres. In the left panel, water, ions and counterions are shown as light grey field; in the right panel, water molecules are depicted as transparent light blue spheres, some Na^+ and Cl^- ions are shown as purple and green spheres, respectively.

Table 2 Main characteristics of the spherical SAMul micelles as obtained from multiscale molecular simulations. N_{agg} = aggregation number; D_m = diameter; ψ_s = surface electrostatic potential; and ζ = zeta potential

Compound	N_{agg}	D_m (nm)	ψ_s (mV)	ζ (mV)
C_{16}-DAPMA	16 ± 2	6.0 ± 0.3	172.4	50.2
C_{16}-SPD	13 ± 1	6.3 ± 0.1	153.3	45.1
C_{16}-SPM	10 ± 1	5.8 ± 0.2	144.6	41.8

forms more tightly packed micelles than C_{16}-SPD, which in turn is more densely packed than C_{16}-SPM. As suggested from experiment, the hydrophobic C_{16} chain struggles to bring together the more highly charged SPM ligands. As a result of the decrease in N_{agg} for C_{16}-SPM, the electrostatic potential ψ_s also decreases, leading to simulated zeta potentials (ζ, Table 2) in good agreement with the experimental data (Table 1), with C_{16}-DAPMA > C_{16}-SPD > C_{16}-SPM.

The ability of SAMul nanostructures to bind polyanions was then tested experimentally. DNA binding was assessed using an ethidium bromide (EthBr) displacement assay[18] in which the compounds displace EthBr from calf thymus DNA, as monitored by fluorimetry. Heparin binding was monitored by UV-Vis spectroscopy using our recently introduced Mallard Blue (MalB) dye in a competition assay.[19] All assays were performed in triplicate. These simple, rapid approaches allowed us to determine CE_{50} values (cation : anion charge excess at which 50% of dye is displaced). These can be converted into EC_{50} values (effective concentration of binder at the same point). Under assay conditions, all compounds had good solubility – interactions between cationic ligands and the polyanionic binding partner decrease cation–cation repulsion at the micellar surface (see below for further discussion).

From these rapid assays, it was found (Table 3) that the more highly charged C_{16}-SPM ligand appears to be the optimal DNA binder with low CE_{50} and EC_{50} values, whereas C_{16}-SPD and C_{16}-DAPMA are less effective. Interestingly, although C_{16}-DAPMA and C_{16}-SPD have the same ligand charge (+2), C_{16}-DAPMA is a slightly better DNA binder. In contrast, for heparin binding,

Table 3 DNA and heparin binding parameters: CE_{50} (cation : anion charge excess at which 50% of indicator dye is displaced from its complex) and EC_{50} (effective concentration at which 50% of dye is displaced)

		C_{16}-DAPMA (+2)	C_{16}-SPD (+2)	C_{16}-SPM (+3)
CE_{50}	DNA	5.0 ± 0.1	6.0 ± 0.3	4.3 ± 0.1
	Heparin	0.69 ± 0.05	0.34 ± 0.05	0.49 ± 0.01
$EC_{50}/\mu M$	DNA	10.1 ± 0.1	11.9 ± 0.5	5.7 ± 0.1
	Heparin	37 ± 3	19 ± 3	17.5 ± 0.3

C_{16}-SPD is the most charge-efficient binder as measured by its CE_{50} value, significantly outperforming C_{16}-DAPMA, even though the latter compound was the slightly better DNA binder and both systems have the same nominal charge. C16-SPD even performs better than more highly charged C_{16}-SPM in terms of its CE_{50} value. Although these differences are relatively small, they were reproducible and outside of error range – as such, they provide some hint that heparin and DNA behave differently when faced with these SAMul nanostructures as binding partners.

All of the reported EC_{50} values (Table 3) were below the CMC values of these compounds (Table 1). Polyanions can assist self-assembly by limiting electrostatic repulsion on the cationic SAMul surface.[20] This agrees with the observation that all compounds showed excellent solubility in polyanion-binding assays, unlike in their absence. It should also be noted that the lineshapes for these binding assays are sigmoidal (Fig. 3) and can be divided into three regions: (i) non-assembled binder initially struggles to displace polyanion-binding dye, (ii) at a critical concentration, binding occurs and dye displacement is activated (iii) the system saturates and no further dye is displaced. The onset of region (ii) allows us to estimate apparent critical aggregation concentration (CAC) values in the presence of the polyanions – see ESI† for full data. These observations are consistent with a system that only self-assembles and binds polyanions at a critical concentration. It is also clear that while self-assembly evidently assists multivalent binding, the converse is also true, and multivalent binding can considerably assist self-assembly – reflecting the dynamic nature of these SAMul nanostructures.

We were somewhat surprised by the DNA/heparin selectivity differences reported above, as we had anticipated that the polyanions would bind to the most highly charged systems best,
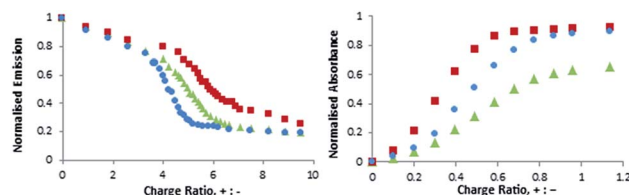

Fig. 3 Titration curves for EthBr (left, DNA binding) and MalB (right, heparin binding) displacement. For DNA binding: [DNA] = 4 μM (per base), [EthBr] = 5.07 μM, buffer: 2 mM HEPES, 0.05 mM EDTA, 150 mM NaCl. For heparin binding: [heparin] = 27 μM (per disaccharide unit), [MalB] = 25 μM, buffer: Tris HCl 10 mM, 150 mM NaCl. Blue = C_{16}-SPM, red = C_{16}-SPD, green = C_{16}-DAPMA.

and that both polyanions would exhibit similar orders of preference. As such, we therefore used ITC to further validate the data. These experiments are complex, as there are many near-simultaneous processes which are difficult to deconvolute: (i) non-assembled ligand binding to polyanion, (ii) ligand self-assembly, (iii) self-assembled ligands binding to polyanion, and (iv) further nanoscale assembly. Nonetheless, we reasoned that we could obtain useful thermodynamic data for the overall binding process which would still be informative (Table 4) and would provide insight into the impact of the presence of the polyanion on the self-assembly of the ligands. In particular, we reasoned that comparing the data with that obtained for the self-assembly of the ligands in the absence of polyanion (Table 1) should allow us to isolate the thermodynamic contributions which are a direct result of ligand–polyanion interactions.

The method was based on titrating the ligand into the polyanion, and therefore allowed us to determine polyanion-modified critical aggregation concentrations (CACs). Interestingly, these modified CAC values had good agreement with those determined from the dye displacement assay (see ESI†), which would suggest good comparability between our different binding assay approaches. Furthermore, ITC allowed us to elucidate the thermodynamic parameters for SAMul self-assembly in the presence of polyanion. By comparing these thermodynamics of aggregation in the presence (ΔH_{agg}, $T\Delta S_{agg}$ and ΔG_{agg}, Table 4) and absence (ΔH_{mic}, $T\Delta S_{mic}$ and ΔG_{mic}, Table 1) of polyanion, we estimate the difference to represent the effective binding between the SAMul nanostructures and the polyanion (e.g. $\Delta H_{bind} = \Delta H_{agg} - \Delta H_{mic}$) (Table 4). This simple approach allows us to extract and quantify the effective change in solution thermodynamics induced by the polyanion.

Table 4 Thermodynamic parameters of aggregation (ΔG_{agg}, $T\Delta S_{agg}$ and ΔG_{agg}) and critical aggregation concentrations (CACs) in the presence of polyanion as obtained from ITC measurements at 298 K in a 30 µM solution of DNA or heparin at 150 mM NaCl. Binding parameters ΔH_{bind}, $T\Delta S_{bind}$, and ΔG_{bind} are defined as the difference between parameters for aggregation in the presence and absence of polyanion, respectively (e.g., $\Delta H_{bind} = \Delta H_{agg} - \Delta H_{mic}$)

		C_{16}-DAPMA (+2)	C_{16}-SPD (+2)	C_{16}-SPM (+3)
CAC (with polyanion)/µM	DNA	6.1	9.8	3.4
	Heparin	13.6	7.2	9.8
ΔH_{agg}/kJ mol^{-1}	DNA	−12.2	−12.5	−15.0
	Heparin	−12.8	−13.5	−11.0
$T\Delta S_{agg}$/kJ mol^{-1}	DNA	17.6	16.2	16.0
	Heparin	15.0	15.9	17.6
ΔG_{agg}/kJ mol^{-1}	DNA	−29.8	−28.7	−31.0
	Heparin	−27.8	−29.4	−28.6
ΔH_{bind}/kJ mol^{-1}	DNA	−1.4	−3.9	−6.6
	Heparin	−1.9	−4.9	−2.6
$T\Delta S_{bind}$/kJ mol^{-1}	DNA	2.9	0.4	0.7
	Heparin	0.3	0.0	2.3
ΔG_{bind}/kJ mol^{-1}	**DNA**	**−4.3**	**−4.2**	**−7.3**
	Heparin	**−2.2**	**−4.9**	**−4.9**

Pleasingly, the ITC data in terms of apparent binding affinity (ΔG_{bind}, bold, Table 4) were in broad agreement with the trends obtained from the dye displacement assays. Once again, C_{16}-SPM was the most effective DNA binder (ΔG_{bind}), and C_{16}-SPD was the most effective heparin binder, especially if the ΔG_{bind} values are normalised per charge (C_{16}-SPD, −2.45 kJ mol^{-1}; C_{16}-SPM, −1.63 kJ mol^{-1}). Furthermore, as in the dye displacement assays, for DNA binding C_{16}-DAPMA > C_{16}-SPD, whereas for heparin binding C_{16}-SPD > C_{16}-DAPMA. Although the thermodynamic differences are relatively small, they are in agreement with the results of the dye displacement assay, supporting the view that specific binding preferences are able to influence the simple ion–ion interactions (which provide the bulk of the binding affinity) in order to generate different selectivity from different polyanions. As such, the ITC data support the view that ligand choice directs polyanion selectivity in this system.

Considering the data in more detail, it is evident that much of the difference in binding appears to be caused by the ability of these polyanions to influence the aggregation of the SAMul ligand displays (ΔG_{agg}, italics, Table 4). In the presence of DNA, the magnitude of ΔG_{agg} for C_{16}-SPM is greater than for the other two ligands, whereas in the presence of heparin, it is C_{16}-SPD which has the largest ΔG_{agg} value – this is also reflected in the apparent CACs in the presence of each of these polyanions. As such, we reason the specifics of the ligand–polyanion interaction can directly influence the ability of the nanostructures to assemble and hence, as a result, exhibit high-affinity SAMul binding.

In order to provide greater insight into the binding interface between the self-assembled nanostructure and the polyanions we once again turned to multiscale simulations. We brought together the SAMul nanostructures as optimised in the absence of polyanion with the polyanions themselves in order to probe the binding interface. Clearly this assumes that the nanostructures do not significantly change in the presence of the polyanion, which is a limitation on the method, but it provides the only tractable approach for simulating the interactions between these SAMul displays and polyanions in order to provide some insight into the thermodynamics of the nanoscale binding interface.

We note that in reality, multiple DNA helices or heparin chains will contact a single micelle. Indeed, this is supported by DLS data (Table S3†) recorded on the complexes formed between these cationic micelles and either heparin or DNA. These DLS data clearly indicate the formation of larger ill-defined aggregates (ca. 100–300 nm in diameter) on binding. The DLS data also provided further support for the binding preferences reported above, with zeta potentials suggesting that C_{16}-SPM was most effective at neutralising the negative charge of DNA, while heparin binding reduced the cationic charge of C_{16}-SPD more than either of the other ligands.

It is important to consider whether the cationic micelles actually remain intact during the polyanion binding process, as there is a possibility that significant reorganisation could occur. To probe this experimentally, we employed transmission electron microscopy (TEM) to visualise the morphologies formed when the self-assembled nanostructures bind to polyanionic

heparin (Fig. 4). In agreement with similar literature studies on related systems[10b,11] the micelles remained remarkably intact, and were organised into hierarchical nanoscale arrays. We suggest this is a result of close packing interactions between the spherical micellar polycations and the linear polyanions. As such, we are confident that the micelles do indeed remain intact on binding, and this supports our suggested methodological approach for computational modelling in which the pre-formed micelle is brought into contact with a polyanion chain in order to determine the fundamental binding interactions.

We therefore reason, with this experimental support from TEM, that our modelling approach which contacts a single micelle with a single polyanion is a valid methodology for gaining insight into the fundamental forces responsible for the primary binding event. In this way, we were interested to determine whether the thermodynamic insights obtained would show broad agreement with our experimental observations of binding. Obviously, understanding the further hierarchical assembly event is more complex, and was beyond the scope of this study, which was instead focussed on the differences induced by different ligands at the initial polyanion binding interface.

For DNA binding (Fig. 5, top), the C_{16}-SPM micelles contain 10 SPM residues, 9 of which effectively contact DNA (a parameter we define as N_{eff}), resulting in a charge-normalized binding free energy (per-effective-residue) ΔG^* of -14.32 kJ mol^{-1}. Conversely, C_{16}-SPD and C_{16}-DAPMA nanostructures only use 7 and 8 (out of 13 and 16) SPM residues, respectively, to bind DNA. For C_{16}-SPD and C_{16}-DAPMA, the per-effective-residue interactions were lower, with ΔG^* values of -9.76 and -10.80 kJ mol^{-1}, respectively. The simulated ΔG^* values therefore follow the same trend as the experimental CE$_{50}$ values and ITC data: C_{16}-SPM > C_{16}-DAPMA > C_{16}-SPD.

For heparin binding (Fig. 5, bottom), the micelles formed by C_{16}-SPD engage 12 out of 13 available ligands in productive binding, resulting in charge-normalized ΔG^* of -14.98 kJ mol^{-1}. However, C_{16}-DAPMA and C_{16}-SPM assemblies only exploit 9/16 and 6/10 ligands, giving ΔG^* values of -8.65 and -11.97 kJ mol^{-1}, respectively. The predicted ΔG^* values are thus in agreement with the trend of experimental data: C_{16}-SPD > C_{16}-SPM > C_{16}-DAPMA.

To understand why polyanions appear to have different selectivities towards SAMul nanostructures, we then deconvoluted these overall ΔG^* values into enthalpic (ΔH^*) and entropic ($-T\Delta S^*$) components (Fig. 6 and ESI†).
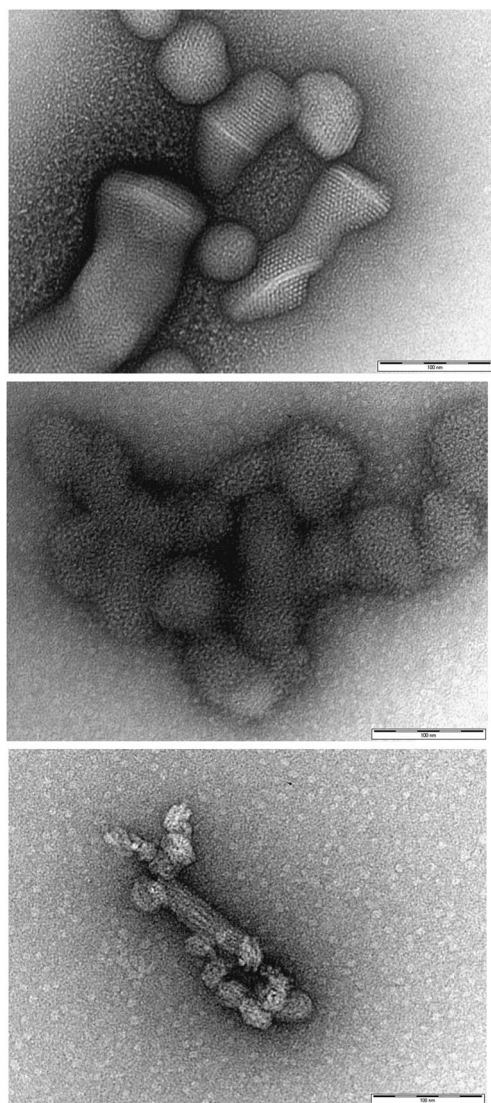

Fig. 4 TEM images of self-assembled micellar nanostructures binding to heparin to yield a hierarchically organised self-assembled nanoscale aggregate and supporting the view that self-assembled micelles remain stable under polyanion binding conditions: (top) C_{16}-DAPMA, (middle) C_{16}-SPD, (bottom) C_{16}-SPM. All scale bars are 100 nm.
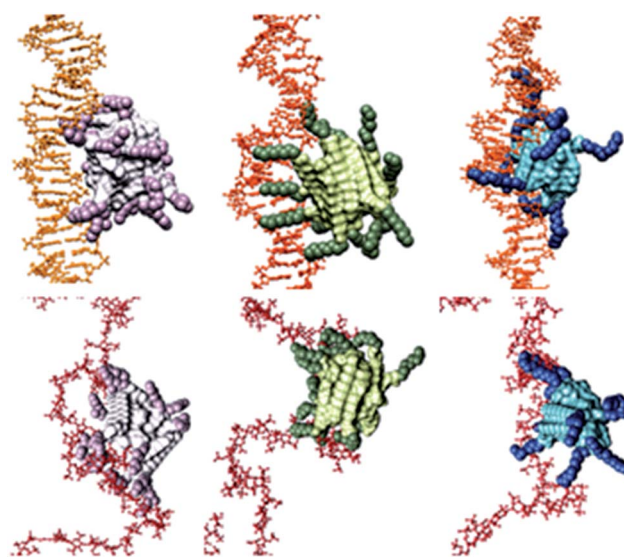

Fig. 5 Equilibrated atomistic molecular dynamics (MD) simulation snapshots of SAMul micelles binding DNA (upper panel, orange) and heparin (lower panel, firebrick). In both panels, from left to right: C_{16}-DAPMA (light grey (C_{16}) and plum (DAPMA)), C_{16}-SPD (lime green (C_{16}) and forest green (SPD)), and C_{16}-SPM (steel blue (C_{16}) and navy blue (SPM)). Hydrogen atoms, water molecules, ions and counterions are not shown for clarity.
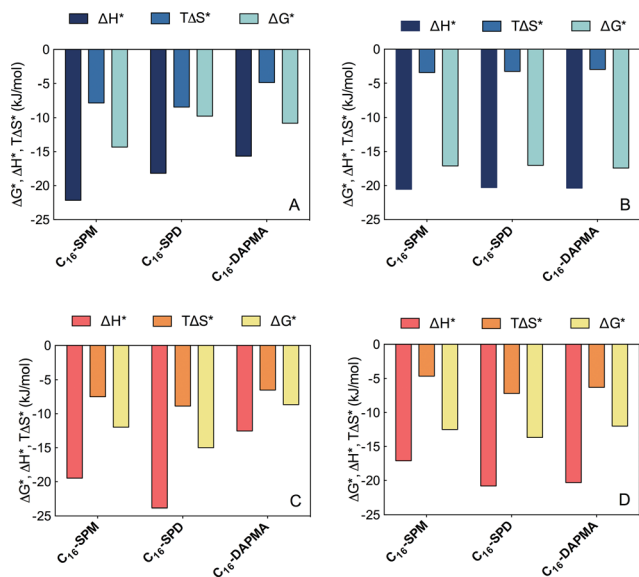
Fig. 6 Charge-normalized per-residue effective free energy of binding (ΔG^*), and enthalpic (ΔH^*) and entropic ($T\Delta S^*$) components for: (A) each SAMul micelle ligand-type complexed with DNA; (B) DNA-bases complexed with each of the SAMul micelles; (C) each SAMul micelle ligand-type complexed with heparin; (D) heparin sugars complexed with each of the SAMul micelles.

For DNA binding (Fig. 5, upper panel) considered from the viewpoint of each effective SAMul cationic charge (Fig. 6A), the flexible C_{16}-SPM (3+) ligands can enthalpically overcompensate the significant entropic cost associated with their organisation on binding DNA. In part, this is due to the greater reduction in cation–cation repulsions at the SAMul surface of C_{16}-SPM on DNA binding, which in turn will assist self-assembly. The other two less-charged ligands have less enthalpic gain and bind less well – in full agreement with the experimental ITC data (Table 4). The slightly more rigid C_{16}-DAPMA suffers less entropic penalty than C_{16}-SPD on binding, as it does not reorganise, slightly favouring its DNA binding over C_{16}-SPD. Once again this is in agreement with ITC data (Table 4).

Applying the same analysis, but from the viewpoint of each anionic DNA charge involved at the binding interface (Fig. 6B), ΔG^*, ΔH^* and $T\Delta S^*$ are practically independent of the choice of ligand – *i.e.*, from the perspective of DNA, all interactions are equally good. The selectivity of the SAMul micelles towards DNA can thus be ascribed only to the optimization of the ligands – as such DNA appears to be a *shape-persistent*[21] polyanion which will simply bind to, and organise the SAMul display with which it is presented.

For heparin binding (Fig. 6, lower panel), considered from the viewpoint of each effective SAMul cationic charge (Fig. 5C), the enthalpic gain when C_{16}-SPD reorganises to optimise its interactions is greater than for C_{16}-DAPMA and also greater than for C_{16}-SPM – in broad agreement with the ITC data (ΔH_{bind}, Table 4). It appears that C_{16}-SPM is less effective at binding the more open surface of heparin in terms of enthalpic gain than it was for DNA. Although the entropic penalty of binding C_{16}-DAPMA is, as for DNA binding, less than that of the more flexible C_{16}-SPD, it is in this case outweighed by the

enthalpic term. As such, C_{16}-SPD emerges as the optimal system for heparin binding, in agreement with ITC (ΔG_{bind}, Table 4).

Considered from the viewpoint of each heparin sugar (-2), we also observe different behaviour depending on the ligand. Each heparin residue offsets the entropic cost of binding SPD with a greater enthalpic gain of its own (Fig. 6D). This is in contrast to DNA, where each anion behaved identically, irrespective of the ligand. As such, the more effective binding of C_{16}-SPD induces more effective binding from each residue of the heparin chain *via* an enthalpy/entropy optimisation, mediated through polyanion structural adaptation – *i.e.* heparin is an *adaptive*[21] polyanion, which not only binds to the SAMul display, but importantly, is also able to adapt itself in response.

We believe that these insights, which correlate experimental and simulation data for the challenging problem of polyanion binding hint at fundamental differences through which some discrimination between polyanions may be achieved. Interestingly, even biology struggles to achieve selectivity between DNA and heparin within its proteins – for example many (but not all) DNA/RNA binding proteins also bind to heparin.[22] Clearly understanding the factors which can lead to even small degrees of selectivity between these polyanions, and developing synthetic nanosystems with this capacity, is therefore useful. In this regard, it is worth noting that flexibility has recently been identified as a key factor in heparin binding proteins – which would be supported by the view, expressed here, of this polyanion being an adaptive binding target.[23]

Conclusions

In summary, this paper demonstrates that ligand choice in SAMul displays can have an influence on apparent binding selectivity. As such, electrostatic ion–ion binding depends on structural detail, not only charge density – as confirmed by the complementary experimental methods of competition binding assays and isothermal calorimetry. Of the compounds studied here, C_{16}-SPM is optimal for DNA binding, while C_{16}-SPD is optimal for heparin binding. We note that the polyanions play a role in assisting self-assembly and hence switching on the multivalent binding effect, and suggest that specifics of ligand–polyanion interactions help mediate subtle differences in this overall process. Molecular simulation studies lead us to propose that the shape-persistence (DNA), or adaptability (heparin) of the polyanionic targets help mediate the selectivity of interaction with different ligands. These results provide intriguing insight into molecular recognition processes at nanoscale surfaces and suggest that SAMul can deliver some selectivity in addressing the challenging problem of the 'polyanion world'.

Acknowledgements

Notes and references

1 L. S. Jones, B. Yazzie and C. R. Middaugh, *Mol. Cell. Proteomics*, 2004, **3**, 746–769.

2 R. Srinivas, S. Samanta and A. Chaudhuri, *Chem. Soc. Rev.*, 2009, **38**, 3326–3338.

3 S. M. Bromfield, E. Wilde and D. K. Smith, *Chem. Soc. Rev.*, 2013, **42**, 9184–9185.

4 (a) K. Riehemann, S. W. Schneider, T. A. Luger, B. Godin, M. Ferrari and H. Fuchs, *Angew. Chem., Int. Ed.*, 2009, **48**, 872–897; (b) D. A. Uhlenheuer, K. Petkau and L. Brunsveld, *Chem. Soc. Rev.*, 2010, **39**, 2817–2826.

5 C. Fasting, C. A. Schalley, M. Weber, O. Seitz, S. Hecht, B. Koksch, J. Dernedde, C. Graf, E. W. Knapp and R. Haag, *Angew. Chem., Int. Ed.*, 2012, **51**, 10472–10498.

6 (a) A. Barnard and D. K. Smith, *Angew. Chem., Int. Ed.*, 2012, **51**, 6572–6581; (b) K. Petkau-Milroy and L. Brunsveld, *Org. Biomol. Chem.*, 2013, **11**, 219–232.

7 (a) J. E. Kingery-Wood, K. W. Williams, G. B. Sigal and G. M. Whitesides, *J. Am. Chem. Soc.*, 1992, **114**, 7303–7305; (b) B. S. Kim, D. J. Hong, J. Bae and M. Lee, *J. Am. Chem. Soc.*, 2005, **127**, 16333–16337; (c) M. K. Müller and L. Brunsveld, *Angew. Chem., Int. Ed.*, 2009, **48**, 2921–2924; (d) E. L. Dane, A. E. Ballok, G. A. O'Toole and M. W. Grinstaff, *Chem. Sci.*, 2014, **5**, 551–557.

8 (a) D. J. Welsh and D. K. Smith, *Org. Biomol. Chem.*, 2011, **9**, 4795–4801; (b) D. J. Welsh, P. Posocco, S. Pricl and D. K. Smith, *Org. Biomol. Chem.*, 2013, **11**, 3177–3186.

9 (a) D. Joester, M. Losson, R. Pugin, H. Heinzelmann, E. Walter, H. P. Merkle and F. Diederich, *Angew. Chem., Int. Ed.*, 2003, **42**, 1486–1490; (b) S. P. Jones, N. P. Gabrielson, D. W. Pack and D. K. Smith, *Chem. Commun.*, 2008, 4700–4702; (c) S. P. Jones, N. P. Gabrielson, C.-H. Wong, H.-F. Chow, D. W. Pack, P. Posocco, M. Fermeglia, S. Pricl and D. K. Smith, *Mol. Pharmaceutics*, 2011, **8**, 416–429; (d) A. Barnard, P. Posocco, S. Pricl, M. Calderon, R. Haag, M. E. Hwang, V. W. T. Shum, D. W. Pack and D. K. Smith, *J. Am. Chem. Soc.*, 2011, **133**, 20288–20300; (e) S. K. M. Nalluri, J. Voskuhl, J. B. Bultema, E. J. Boekema and B. J. Ravoo, *Angew. Chem., Int. Ed.*, 2011, **50**, 9747–9751; (f) A. Tschiche, A. M. Staedtler, S. Malhotra, H. Bauer, C. Böttcher, S. Sharbati, M. Calderon, M. Koch, T. M. Zollner, A. Barnard, D. K. Smith, R. Einspanier, N. Schmidt and R. Haag, *J. Mater. Chem. B*, 2014, **2**, 2153–2167; (g) X. Liu, J. Zhou, T. Yu, C. Chen, Q. Cheng, K. Sengupta, Y. Huang, H. Li, C. Liu, Y. Wang, P. Posocco, M. Wang, Q. Cui, S. Giorgio, M. Fermeglia, F. Qu, S. Pricl, Y. Shi, Z. Liang, P. Rocchi, J. J. Rossi and L. Peng, *Angew. Chem., Int. Ed.*, 2014, **53**, 11822–11827.

10 (a) K. Rajangam, H. A. Behanna, M. J. Hui, X. Han, J. F. Hulvat, J. W. Lomasney and S. I. Stupp, *Nano Lett.*, 2006, **6**, 2086–2090; (b) A. C. Rodrigo, A. Barnard, J. Cooper and D. K. Smith, *Angew. Chem., Int. Ed.*, 2011, **50**, 4675–4679; (c) S. M. Bromfield, P. Posocco, C. W. Chan, M. Calderon, S. E. Guimond, J. E. Turnbull, S. Pricl and D. K. Smith, *Chem. Sci.*, 2014, **5**, 1484–1492; (d) G. L. Montalvo, Y. Zhang, T. M. Young, M. J. Costanzo, K. B. Freeman, J. Wang, D. J. Clements, E. Magavern, R. W. Kavash, R. W. Scott, D. H. Liu and W. F. DeGrado, *ACS Chem. Biol.*, 2014, **9**, 967–975.

11 S. M. Bromfield and D. K. Smith, *J. Am. Chem. Soc.*, 2015, **137**, 10056–10059.

12 L. Chiappisi, I. Hoffmann and M. Gradzielski, *Soft Matter*, 2013, **9**, 3896–3909.

13 (a) A. Perico and A. Ciferri, *Chem.–Eur. J.*, 2009, **15**, 6312–6320; (b) D. Li and N. J. Wagner, *J. Am. Chem. Soc.*, 2013, **135**, 17547–17555; (c) M. S. Sulatha and U. Natarajan, *J. Phys. Chem. B*, 2015, **119**, 12526–12539.

14 For a review see: K. Kogej, *Adv. Colloid Interface Sci.*, 2010, **158**, 68–83.

15 K. Esumi and M. Ueno, *Structure-Performance Relationships in Surfactants*, Marcel Dekker, New York, 2003.

16 M. C. A. Stuart, J. C. van de Pas and J. B. F. N. Engberts, *J. Phys. Org. Chem.*, 2005, **18**, 929–934.

17 P. Posocco, E. Laurini, V. Dal Col, D. Marson, K. Karatasos, M. Fermeglia and S. Pricl, *Curr. Med. Chem.*, 2012, **19**, 5062–5087.

18 (a) B. F. Cain, B. C. Baguley and W. A. Denny, *J. Med. Chem.*, 1978, **21**, 658–668; (b) D. L. Boger, B. E. Fink, S. R. Brunette, W. C. Tse and M. P. Hedrick, *J. Am. Chem. Soc.*, 2001, **123**, 5878–5891.

19 (a) S. M. Bromfield, A. Barnard, P. Posocco, M. Fermeglia, S. Pricl and D. K. Smith, *J. Am. Chem. Soc.*, 2013, **135**, 2911–2914; (b) S. M. Bromfield, P. Posocco, M. Fermeglia, S. Pricl, J. Rodríguez-López and D. K. Smith, *Chem. Commun.*, 2013, **49**, 4830–4832.

20 (a) A. J. Konop and R. H. Colby, *Langmuir*, 1999, **15**, 58–65; (b) H. Schiessel, M. D. Correa-Rodriguez, S. Rudiuk, D. Baigl and K. Yoshikawa, *Soft Matter*, 2012, **8**, 9406–9411.

21 S. M. Bromfield, P. Posocco, M. Fermeglia, J. Tolosa, A. Herreros-López, S. Pricl, J. Rodriguez-López and D. K. Smith, *Chem.–Eur. J.*, 2014, **20**, 9666–9674.

22 For a range of examples see: (a) K. Ishii, S. Futaki, H. Uchiyama, K. Nagasawa and T. Andoh, *Biochem. J.*, 1987, **241**, 111–119; (b) J. Dudas, G. Ramadori, T. Knittel, K. Neubauer, D. Raddatz, K. Egedy and I. Kovalszky, *Biochem. J.*, 2000, **350**, 245–251; (c) H. Ma, V. Leveque, A. De Witte, W. X. Li, T. Hendricks, S. M. Clausen, N. Cammack and K. Klumpp, *Virology*, 2005, **332**, 8–15.

23 (a) J. A. Huntington, *Biochim. Biophys. Acta, Proteins Proteomics*, 2012, **1824**, 246–252; (b) K.-W. Jeong, M.-C. Jeong, B. Jin and Y. Kim, *Biochemistry*, 2013, **52**, 8823–8832.